

Ferromagnetic ordering along the hard axis in the Kondo lattice YbIr_3Ge_7

Binod K. Rai^{1,*}, Macy Stavinoha^{2,*}, J. Banda³, D. Hafner³, Katherine A. Benavides⁴,

D. A. Sokolov³, Julia Chan⁴, M. Brando³, C.-L. Huang², and E. Morosan^{1,2}

¹ Department of Physics and Astronomy, Rice University, Houston, TX 77005 USA

² Department of Chemistry, Rice University, Houston, TX 77005 USA

³ Max Planck Institute for Chemical Physics of Solids,
Nöthnitzer Strasse 40, Dresden, 01187, Germany

⁴ Department of Chemistry, University of Texas at Dallas, Richardson, TX 75080, USA

(Dated: January 10, 2019)

Ferromagnetic Kondo lattice compounds are far less common than their antiferromagnetic analogs. In this work, we report the discovery of a new ferromagnetic Kondo lattice compound, YbIr_3Ge_7 . Like almost all ferromagnetic Kondo lattice systems, YbIr_3Ge_7 shows magnetic order with moments aligned orthogonal to the crystal electric field (CEF) easy axis. YbIr_3Ge_7 is unique in that it is the only member of this class of compounds that crystallizes in a rhombohedral structure with a trigonal point symmetry of the magnetic site, and it lacks broken inversion symmetry at the local moment site. AC magnetic susceptibility, magnetization, and specific heat measurements show that YbIr_3Ge_7 has a Kondo temperature $T_K \approx 14$ K and a Curie temperature $T_C = 2.4$ K. Ferromagnetic order occurs along the crystallographic [100] hard CEF axis despite the large CEF anisotropy of the ground state Kramers doublet with a saturation moment along [001] almost four times larger than the one along [100]. This implies that a mechanism which considers the anisotropy in the exchange interaction to explain the hard axis ordering is unlikely. On the other hand, the broad second-order phase transition at T_C favors a fluctuation-induced mechanism.

Various competing ground states in Kondo lattice (KL) systems, governed by the delicate balance between the Ruderman-Kittel-Kasuya-Yosida (RKKY) exchange interaction and on-site Kondo effect, have gained great interest for over three decades [1–3]. These two interactions usually result in antiferromagnetic (AFM) order with a dense KL metallic ground state. The balance between Kondo and RKKY interactions can be tuned by applying non-thermal parameters such as pressure, magnetic field, or chemical doping, resulting in non-Fermi liquid behavior near a quantum critical point (QCP) where the AFM transition temperature is suppressed to absolute zero, or other quantum collective phenomena emerge including unconventional superconductivity [4–6].

Among known KLs, the number of compounds that shows AFM order greatly surpasses that of the ferromagnetically ordered compounds [7–9]. Thus, in stark contrast to the AFM counterpart, in-depth theoretical work to describe ferromagnetic (FM) KL compounds is largely missing [10, 11]. Recently Ahamed et al. [8] suggested that broken inversion symmetry at the local moment site could promote FM order in KLs. While this scenario is possible for most of the Ce- and Yb-based FM KL compounds, including CeTiGe_3 [12], YbNiSn [13], YbPtGe [14], YbRhSb [15], YbPdSi [16], and the most heavily studied FM KLs CeAgSb_2 [17–21], CeRuPO [22–24] and YbNi_4P_2 [25], it does not apply to systems *with* inversion symmetry like $\text{Yb}(\text{Rh}_{0.73}\text{Co}_{0.27})_2\text{Si}_2$ [26, 27] and YbCu_2Si_2 [28, 29]. Moreover, it has been theoretically and experimentally found that the FM phase is inherently unstable, either towards a first-order phase transition [30] or towards inhomogeneous magnetic phases [31]. Thus, the FM QCP either does not exist or is masked by

other phases. Only in the case of YbNi_4P_2 , FM order occurs via a second-order phase transition upon chemical substitution in $\text{YbNi}_4(\text{P}_{1-x}\text{As}_x)_2$ [32]. The presence of a FM QCP in this system has been attributed to its quasi-1D structure [25, 32]. Thus, in order to develop the theory surrounding FM KL systems in general, and experimentally realize new FM QCPs in particular, new FM KL compounds are called for.

In compounds with strong crystal electric field (CEF) effects, the CEF-induced anisotropy determines the direction of easy and hard magnetization axes in the paramagnetic (PM) state. Interestingly, in all of the FM KL compounds mentioned above, with the exception of CeTiGe_3 and YbCu_2Si_2 , this CEF anisotropy competes with the RKKY interaction and results in magnetic ordering along the axis *orthogonal* to the CEF easy axis [17, 22, 25, 27, 32, 33]. Even more astonishing is the fact that the FM hard axis ordering appears to be a general trait of FM KL systems, as of yet unexplained. [9].

In this paper, we report the discovery of a new FM KL compound YbIr_3Ge_7 with $T_C = 2.4$ K. In line with the above empirical observation, spontaneous magnetization occurs along the hard CEF axis. However, YbIr_3Ge_7 is unique among FM KLs because it is the only such compound crystallizing in a rhombohedral lattice, and it does not show broken inversion symmetry at the local moment site. Recently, we discovered a series of Ce- and Yb-based compounds in this 1-3-7 structural family, including YbRh_3Si_7 [34], CeIr_3Ge_7 [35, 36], and YbIr_3Si_7 [37]. Among these compounds, YbRh_3Si_7 and YbIr_3Si_7 are KL compounds with the former proposed to order antiferromagnetically below 7.5 K based on neutron scattering, and the latter showing ferromagnetic correlations

below 4 K, with the moments ordered along the hard CEF axis in both. In contrast, CeIr_3Ge_7 shows AFM order along the easy CEF axis at a remarkably low temperature $T_N = 0.63$ K, in the absence of Kondo screening or frustration. Although chemically and structurally similar, the balance between CEF effects, Kondo screening, and RKKY interactions in these systems differ drastically. Thus, this family of compounds presents an opportunity to study the delicate competition among these interactions and the resulting ground states.

Single crystals of YbIr_3Ge_7 were grown using Ge self-flux, as described in earlier publications [38, 39]. The purity and crystal structure were identified by single crystal and powder x-ray diffraction analysis (Tables S1 and S2 and Fig. S1 in the Appendix). YbIr_3Ge_7 crystallizes in the ScRh_3Si_7 structure type [40, 41] with lattice parameters $a = 7.8062(10)$ Å and $c = 20.621(5)$ Å. The stoichiometry determined by free variable refinement of the occupancies is $\text{YbIr}_3\text{Ge}_{7-\delta}$ where $\delta = 0.3$. The crystals were oriented along the [100] and [001] hexagonal axes using a back-scattering Laue camera. Room temperature powder x-ray diffraction data were collected using a Bruker D8 diffractometer with $\text{Cu K}\alpha$ radiation, with additional room temperature single crystal x-ray diffraction performed using a Bruker D8 Quest Kappa single crystal x-ray diffractometer equipped with an $I\mu\text{S}$ micro-focus source, a HELIOS optics monochromator, and a CMOS detector. The anisotropic DC magnetic susceptibility M/H and magnetization data were measured using a Quantum Design (QD) Magnetic Property Measurement System (MPMS) with an applied magnetic field up to 7 T. AC susceptibility was measured with a QD MPMS with a modulation field amplitude $\mu_0 H_{\text{ac}} = 1$ mT at a frequency of 113.7 Hz. AC susceptibility measurements at 20 mK were performed using an Oxford Instruments dilution refrigerator. Specific heat and electrical transport measurements were performed in a QD Physical Property Measurement System.

In YbIr_3Ge_7 , the Yb atom occupies a trigonal point symmetry ($\bar{3}$), and the $J = 7/2$ energy levels are split by the CEF in four Kramers doublets. While the CEF energy levels for the Ce isostructural compound were determined from magnetic susceptibility measurements and calculations [35, 36], the larger angular momentum of the Yb leads to a corresponding Hamiltonian with six parameters in YbIr_3Ge_7 , which can not be fully solved with the data at hand. However, large CEF anisotropy in YbIr_3Ge_7 is evidenced by the linear high-temperature inverse susceptibility $H/(M - M_0)$ shown in Fig. 1a, measured for field $H \parallel [001]$ (blue symbols) and $H \parallel [100]$ (red symbols). The Curie-Weiss fit (solid line) of the average inverse susceptibility (purple) between 400 and 600 K yields the experimental effective moment $\mu_{\text{eff}} = 4.42 \mu_B/\text{Yb}$, close to the calculated value $4.54 \mu_B/\text{Yb}$ for Yb^{3+} . The paramagnetic Weiss temperatures along [100] and [001] are both negative,

$\theta_{\text{W}}^{[100]} = -400$ K and $\theta_{\text{W}}^{[001]} = -70$ K, and yield a first CEF parameter $B_2^0 = -1.6$ meV [42], which is a measure of the strength of the CEF anisotropy. Deviations from linearity below 300 K indicate that CEF splitting exceeds this temperature range, similar to the large splitting observed in the Ce analog [35, 36].

Further insight into the low-temperature magnetic properties of YbIr_3Ge_7 comes from the magnetic AC susceptibility shown in Fig. 1b. AC susceptibility measurements reveal spontaneous magnetization below $T_C = 2.4$ K for $H \parallel [100]$, indicative of ferromagnetic order. This is indeed consistent with the transition moving up in temperature (vertical arrows, Fig. 1b) with increasing applied field. At zero field the susceptibilities measured with $H_{\text{ac}} \parallel [100]$ and $H_{\text{ac}} \parallel [001]$ cross each other at a temperature just above T_C . This behavior is similar to that of the heavy fermion ferromagnet YbNi_4P_2 and of all other KL ferromagnets which order along the hard direction [9, 32].

The temperature-dependent electrical resistivity in YbIr_3Ge_7 is typical of dense KL systems, as shown in Fig. 2. Metallic behavior with a positive resistivity coefficient ($d\rho/dT > 0$) is observed between 300 K and 40 K. On further cooling, the resistivity shows a local minimum around 35 K, followed by a $-\ln T$ increase (dashed line) down to a coherence maximum around 6 K for $H = 0$ (red open symbols, Fig. 2), reflecting the incoherent Kondo scattering behavior. A drop in resistivity is seen as the temperature is further lowered through a magnetic phase transition around 2.4 K, as shown more clearly in a derivative plot in Fig. S2. The resistivity in applied magnetic field $\mu_0 H = 9$ T (full symbols, Fig. 2) shows the partial suppression of the Kondo effect and the FM fluctuations as the logarithmic increase disappears and the local maximum moves up in temperature.

A closer look at the ordered state with $T = 1.8$ K magnetization isotherms (Fig. 3) confirms the $H \parallel [100]$ ferromagnetic ordering (red closed circles), while the magnetization shows crossing around $\mu_0 H = 0.1$ T when $H \parallel [001]$ (blue, open symbols) and $H \parallel [100]$ (red, full symbols): small spontaneous magnetization (left inset) is observed for $H \parallel [100]$, while the $H \parallel [001]$ $M(H)$ is nearly linear at low H. A small magnetization hysteresis with a coercive field ≈ 6 mT is revealed at 20 mK in AC susceptibility measurements with $H \parallel [100]$, best illustrated in the $\chi'(H)$ plot (right inset). These features indicate that the FM ordering occurs with moments along the CEF hard direction [100]. The field along the CEF easy direction [001] rotates the moments to saturation without increasing much above 5 T, suggesting the absence of a relevant Van Vleck contribution [27]. The saturation magnetization of the ground state Kramers doublet for $H \parallel [100]$ is reached at very small fields with $M_{[100]}^{\text{sat}} \approx 0.41 \mu_B$ whereas for $H \parallel [001]$ is reached at fields larger than 4 T with $M_{[001]}^{\text{sat}} \approx 1.55 \mu_B$. This yields

a relatively large anisotropy factor of about 4. Therefore, assuming anisotropic exchange interaction to explain the FM ordering with moments along the CEF hard axis [43] seems unlikely in the case of YbIr_3Ge_7 , because this would necessitate an extremely large anisotropy for the exchange interaction [44].

Further evidence of the FM order in YbIr_3Ge_7 is shown by the specific heat (Fig. 4), marked by the peak at $T_C = 2.4\text{ K}$, consistent with the magnetization and resistivity derivatives (Fig. S2). As $T \rightarrow 0$, an enhanced electronic specific heat coefficient $\gamma_0 \sim \frac{C_p}{T} \approx 300\text{ mJ/mol}\cdot\text{K}^2$ is observed in YbIr_3Ge_7 (red), while the corresponding γ_0 for the non-magnetic analog LuIr_3Ge_7 (black line) is, as expected, $< 5\text{ mJ/mol}\cdot\text{K}^2$. The mass renormalization and the small magnetic entropy release at T_C , $S_{mag} \sim 17\%$ (Fig. 4(b)), suggest Kondo lattice forma-

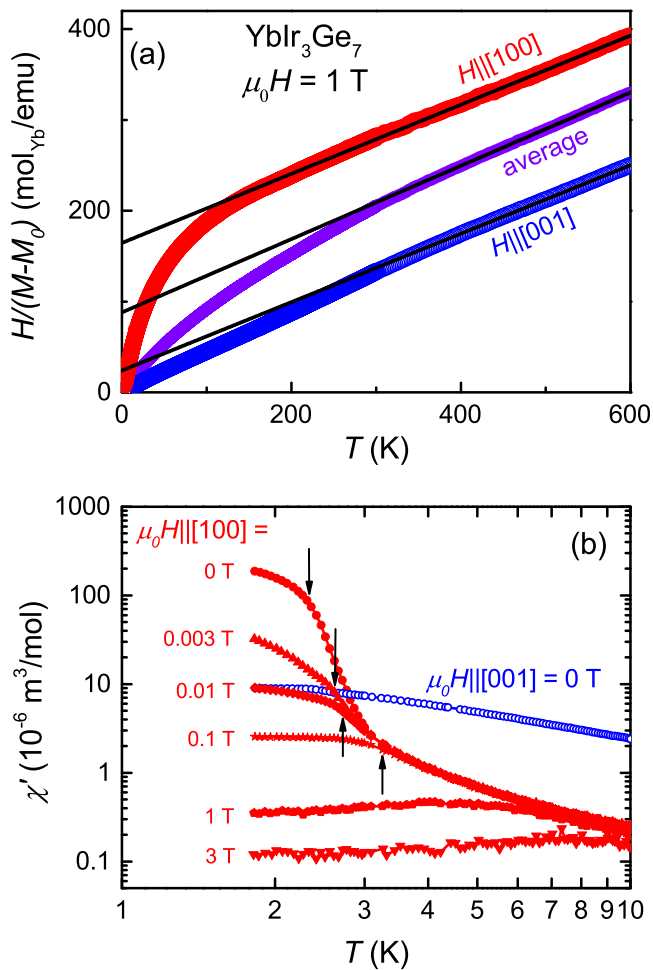


FIG. 1. (a) Inverse magnetic susceptibility $H/(M - M_0)$ vs. T with the polycrystalline average, $M_{avg} = (M_{001} + 2M_{100})/3$ (purple line) and Curie-Weiss fits between $T = 400 - 600\text{ K}$ (solid black lines) (b) Temperature-dependent AC magnetic susceptibility χ' with H_{ac} along [001] (blue open symbols) and along [100] (red closed symbols) with different applied static fields H applied also along [100].

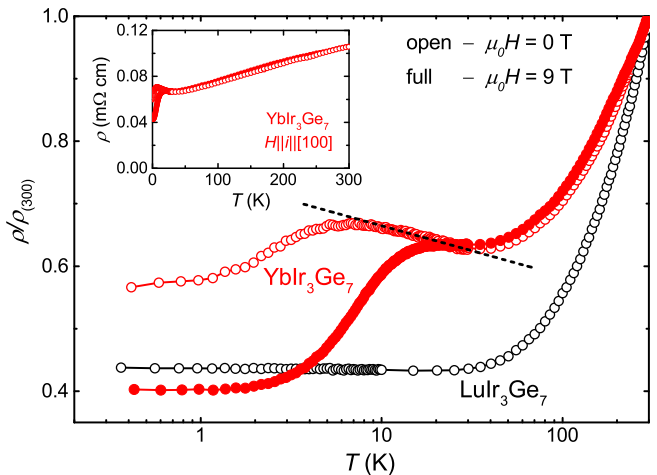


FIG. 2. Scaled temperature-dependent electrical resistivity ρ/ρ_{300} of YbIr_3Ge_7 (red circles) with $\mu_0 H = 0$ (open symbols) and 9 T (closed symbols) for $H \parallel z \parallel [100]$. The nonmagnetic polycrystalline analog LuIr_3Ge_7 is shown with black symbols. The dashed line in the main panel shows a $-\ln T$ increase in $\rho(T)$. The inset shows the absolute resistivity of YbIr_3Ge_7 with $\mu_0 H = 0$ and 9 T

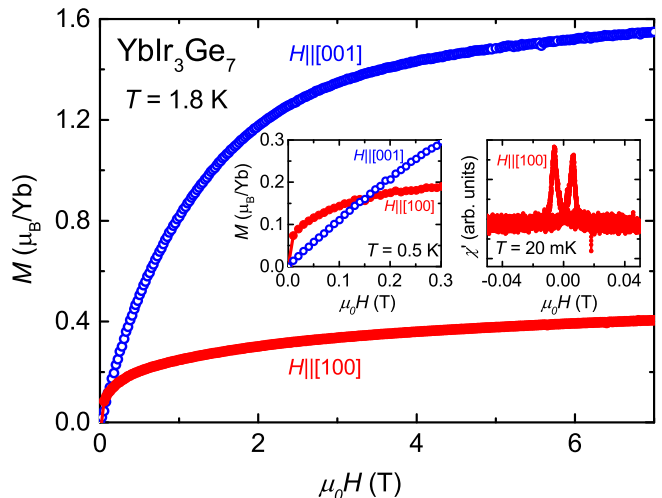


FIG. 3. Magnetization isotherm $M(H)$ at $T = 1.8\text{ K}$ for $H \parallel [100]$ (closed red circles) and $H \parallel [001]$ (open blue circles). Left inset: low field $M(H)$. Right inset: Ferromagnetic hysteresis in the AC susceptibility at 20 mK along $H \parallel [100]$.

tion in YbIr_3Ge_7 , with a Kondo temperature $T_K \sim 14\text{ K}$ estimated from $S_{mag}(0.5 T_K) = 0.5 R \ln 2$. This T_K estimate is in line with the temperature region where the resistivity exhibits Kondo resonance. YbIr_3Ge_7 thus appears to be a rare Yb-based KL ferromagnet with hard axis moment ordering, and the first such compound crystallizing in a rhombohedral lattice.

In Yb-based KLs, the development of FM order away from the CEF easy axis has been revealed in several compounds with different structures, and a wide range of

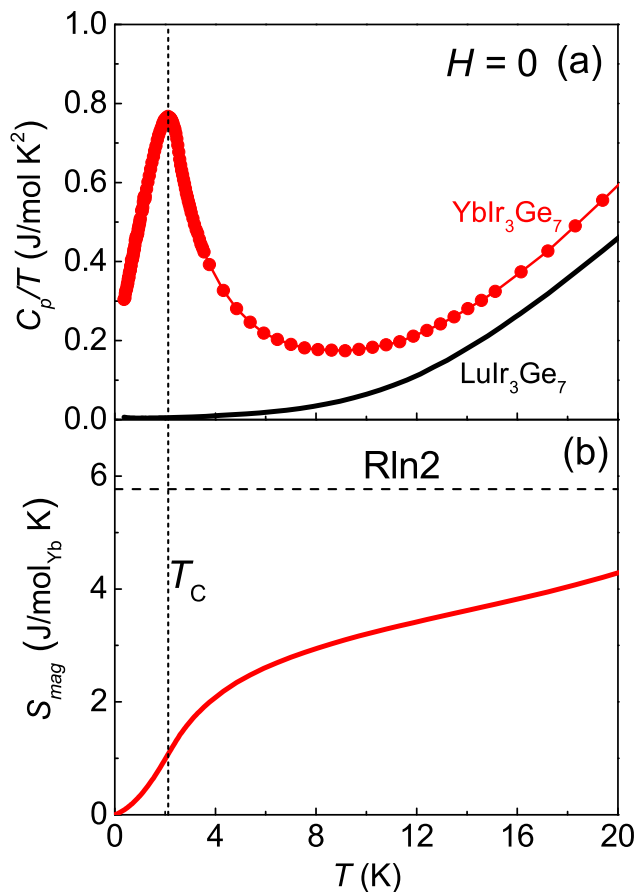


FIG. 4. (a) $H = 0$ specific heat of YbIr_3Ge_7 (red symbols and line) and LuIr_3Ge_7 (black line) (b) Magnetic entropy of YbIr_3Ge_7 with $S_{\text{mag}} = \int_0^T \frac{C_{\text{mag}}}{T} dT$, where $C_{\text{mag}} = C_p(\text{YbIr}_3\text{Ge}_7) - C_p(\text{LuIr}_3\text{Ge}_7)$.

T_C , from 0.15 K in YbNi_4P_2 [25] to 15 K in CeRuPO [22], while T_K ranges from 7 K in CeRuPO [22] up to 30 K in YbRhSb [15]. While YbIr_3Ge_7 has a three-dimensional crystal structure, YbNi_4P_2 is quasi-one-dimensional. This implies that the dimensionality of magnetic interactions and the relative magnitude of the magnetic and Kondo energy scales, *i.e.*, the position in the Doniach phase diagram [1], have little to no effect on the FM order along the hard axis in these Kondo ferromagnets.

Krüger et al. [11] proposed a theoretical model to account for the hard axis ferromagnetic order: they suggested that magnetic order along the hard axis can maximize the phase space for spin fluctuations in the easy plane, leading to a minimum in free energy. This is supported by the broadness of the specific heat peak (Fig. 4), hinting at the presence of fluctuations, but is brought into question by the nature of the magnetic anisotropy in YbIr_3Ge_7 : The presence of an easy axis along c rather than an easy plane does not fit well into this picture. In fact, in the case of CeTiGe_3 [12], which

has a much stronger easy axis anisotropy, the moments do order along the easy axis. Furthermore, a comparison of YbIr_3Ge_7 with the other isostructural Yb compounds is called for: YbIr_3Si_7 [37] and YbRh_3Si_7 [34] are both recently discovered highly anisotropic Kondo lattice systems, with hard axis ferromagnetic correlations in the former, and antiferromagnetic ground state in the latter as suggested by neutron scattering, with a small remanent magnetization of about $0.15 \mu_B/\text{Yb}$ along the [100] direction. Beyond the KLs showing hard axis ordering, several other strongly correlated FMs [9] reveal that magnetic order away from the CEF easy axis is not an exception, but rather a frequent enough occurrence to warrant a thorough theoretical investigation. The "1-3-7" compounds (YbIr_3Ge_7 with ferromagnetic order and YbIr_3Si_7 with ferromagnetic correlations [37], together with the antiferromagnet YbRh_3Si_7 [34]) have the Yb ions in the lowest point symmetry (trigonal) of all these KL compounds. With CEF effects inherently tied to the point symmetry of the magnetic moment, the observation of magnetic order away from the easy axis in different point symmetry cases underlines the difficulty of a generalized theory, which is left to a separate thorough theoretical study.

In conclusion, we report the discovery of a KL compound YbIr_3Ge_7 that shows FM ordering at $T_C = 2.4$ K, with the moment lying along the CEF hard direction. With a rhombohedral crystal lattice, this material expands this class of systems to include a new crystal structure. With relatively small T_C and T_K , YbIr_3Ge_7 is an ideal candidate to study FM QCP by chemical substitution, and to further develop existing theories to explain FM KL compounds.

BKR, MS, CLH, and EM acknowledge support from the Gordon and Betty Moore Foundation EPiQS Initiative through grant GBMF 4417. E.M. acknowledges travel support to Max Planck Institute in Dresden, Germany from the Alexander von Humboldt Foundation Fellowship for Experienced Researchers. This research is funded in part by a QuanEmX grant from ICAM and the Gordon and Betty Moore Foundation through Grant GBMF 5305 to Binod K. Rai. We thank the DFG for financial support from project BR 4110/1-1. JYC acknowledges support from NSF: DMR-1700030.

* These authors contributed equally to this work.

- [1] S. Doniach, *Physica B+C* **91**, 231 (1977).
- [2] G. Stewart, *Reviews of Modern Physics* **73**, 797 (2001).
- [3] H. v. Löhneysen, A. Rosch, M. Vojta, and P. Wölfle, *Reviews of Modern Physics* **79**, 1015 (2007).
- [4] P. Gegenwart, T. Westerkamp, C. Krellner, Y. Tokiwa, S. Paschen, C. Geibel, F. Steglich, E. Abrahams, and Q. Si, *Science* **315**, 969 (2007).
- [5] J. Paglione, T. Sayles, P.-C. Ho, J. Jeffries, and M. Maple, *Nature Physics* **3**, 703 (2007).

- [6] B. Keimer and J. Moore, *Nature Physics* **13**, 1045 (2017).
- [7] M. Brando, D. Belitz, F. M. Grosche, and T. Kirkpatrick, *Reviews of Modern Physics* **88**, 025006 (2016).
- [8] S. Ahamed, R. Moessner, and O. Erten, *Physical Review B* **98**, 054420 (2018).
- [9] D. Hafner, B. K. Rai, J. Banda, K. Kliemt, C. Krellner, J. Sichelschmidt, E. Morosan, C. Geibel, and M. Brando, *arXiv* (2018).
- [10] S. J. Yamamoto and Q. Si, *Proceedings of the National Academy of Sciences* **107**, 15704 (2010).
- [11] F. Krüger, C. Pedder, and A. Green, *Physical review letters* **113**, 147001 (2014).
- [12] V. Fritsch, O. Stockert, C.-L. Huang, N. Bagrets, W. Kitzler, C. Taubenheim, B. Pilawa, S. Woitschach, Z. Huesges, S. Lucas, *et al.*, *The European Physical Journal Special Topics* **224**, 997 (2015).
- [13] P. Bonville, P. Bellot, J. Hodges, P. Imbert, G. Jéhanno, G. Le Bras, J. Hammann, L. Leylekian, G. Chevrier, P. Thuéry, *et al.*, *Physica B: Condensed Matter* **182**, 105 (1992).
- [14] K. Katoh, S. Nakagawa, G. Terui, and A. Ochiai, *Journal of the Physical Society of Japan* **78**, 104721 (2009).
- [15] Y. Muro, Y. Haizaki, M. Kim, K. Umeo, H. Tou, M. Sera, and T. Takabatake, *Physical Review B* **69**, 020401 (2004).
- [16] N. Tsujii, L. Keller, A. Dönni, and H. Kitazawa, *Journal of Physics: Condensed Matter* **28**, 336002 (2016).
- [17] K. Myers, S. Bud'ko, I. Fisher, Z. Islam, H. Kleinke, A. Lacerda, and P. Canfield, *Journal of magnetism and magnetic materials* **205**, 27 (1999).
- [18] G. André, F. Bourée, M. Kolenda, B. Leśniewska, A. Oleś, and A. Szytuła, *Physica B: Condensed Matter* **292**, 176 (2000).
- [19] V. Sidorov, E. Bauer, N. Frederick, J. Jeffries, S. Nakatsuji, N. Moreno, J. Thompson, M. Maple, and Z. Fisk, *Physical Review B* **67**, 224419 (2003).
- [20] S. Araki, N. Metoki, A. Galatanu, E. Yamamoto, A. Thamizhavel, and Y. Ōnuki, *Physical Review B* **68**, 024408 (2003).
- [21] T. Takeuchi, A. Thamizhavel, T. Okubo, M. Yamada, N. Nakamura, T. Yamamoto, Y. Inada, K. Sugiyama, A. Galatanu, E. Yamamoto, *et al.*, *Physical Review B* **67**, 064403 (2003).
- [22] C. Krellner and C. Geibel, *Journal of Crystal Growth* **310**, 1875 (2008).
- [23] C. Krellner, N. Kini, E. Brüning, K. Koch, H. Rosner, M. Nicklas, M. Baenitz, and C. Geibel, *Physical Review B* **76**, 104418 (2007).
- [24] C. Krellner, T. Foerster, H. Jeevan, C. Geibel, and J. Sichelschmidt, *Physical review letters* **100**, 066401 (2008).
- [25] C. Krellner, *New J. Phys.* **13**, 103014 (2011).
- [26] C. Klingner, C. Krellner, M. Brando, C. Geibel, F. Steglich, D. Vyalikh, K. Kummer, S. Danzenbächer, S. Molodtsov, C. Laubschat, *et al.*, *Physical Review B* **83**, 144405 (2011).
- [27] S. Lausberg, A. Hannaske, A. Steppke, L. Steinke, T. Gruner, L. Pedrero, C. Krellner, C. Klingner, M. Brando, C. Geibel, *et al.*, *Physical review letters* **110**, 256402 (2013).
- [28] T. Shimizu, H. Yasuoka, Z. Fisk, and J. L. Smith, *Journal of the Physical Society of Japan* **56**, 4113 (1987).
- [29] N. Tateiwa, T. D. Matsuda, Y. Haga, and Z. Fisk, *Phys. Rev. B* **89**, 035127 (2014).
- [30] D. Belitz, T. R. Kirkpatrick, and T. Vojta, *Physical review letters* **82**, 4707 (1999).
- [31] H. Kotegawa, T. Toyama, S. Kitagawa, H. Tou, R. Yamauchi, E. Matsuoka, and H. Sugawara, *Journal of the Physical Society of Japan* **82**, 123711 (2013).
- [32] A. Steppke, R. Kuchler, S. Lausberg, E. Lengyel, L. Steinke, R. Borth, T. Lühmann, C. Krellner, M. Nicklas, C. Geibel, *et al.*, *Science* **339**, 933 (2013).
- [33] C. Krellner and C. Geibel, in *Journal of Physics: Conference Series*, Vol. 391 (IOP Publishing, 2012) p. 012032.
- [34] B. K. Rai, S. Chikara, X. Ding, I. W. H. Oswald, R. Schönemann, V. Loganathan, A. M. Hallas, H. B. Cao, M. Stavinoha, T. Chen, H. Man, S. Carr, J. Singleton, V. Zapf, K. A. Benavides, J. Y. Chan, Q. R. Zhang, D. Rhodes, Y. C. Chiu, L. Balicas, A. A. Aczel, Q. Huang, J. W. Lynn, J. Gaudet, D. A. Sokolov, H. C. Walker, D. T. Adroja, P. Dai, A. H. Nevidomskyy, C.-L. Huang, and E. Morosan, *Phys. Rev. X* **8**, 041047 (2018).
- [35] B. K. Rai, J. Banda, M. Stavinoha, R. Borth, D.-J. Jang, K. A. Benavides, D. Sokolov, J. Y. Chan, M. Nicklas, M. Brando, *et al.*, *Physical Review B* **98**, 195119 (2018).
- [36] J. Banda, B. Rai, H. Rosner, E. Morosan, C. Geibel, and M. Brando, *Physical Review B* **98**, 195120 (2018).
- [37] M. Stavinoha, W. Phelan, V. Loganathan, N. Carocanales, C. Geibel, C.-L. Huang, and E. Morosan, unpublished.
- [38] J. Remeika, *Solid State Commun.* **34**, 923 (1980).
- [39] B. K. Rai, I. W. Oswald, J. K. Wang, G. T. McCandless, J. Y. Chan, and E. Morosan, *Chemistry of Materials* **27**, 2488 (2015).
- [40] B. Chabot, N. Engel, and E. Parthé, *Acta Crystallographica Section B* **37**, 671 (1981).
- [41] P. Lorenz and W. Jung, *Acta Crystallographica Section E: Structure Reports Online* **62**, i173 (2006).
- [42] G. Bowden, D. S. P. Bunbury, and M. McCausland, *Journal of Physics C: Solid State Physics* **4**, 1840 (1971).
- [43] E. C. Andrade and M. Vojta, *Physical Review B* **90**, 205112 (2014).
- [44] S. Hamann, J. Zhang, D. Jang, A. Hannaske, L. Steinke, S. Lausberg, L. Pedrero, C. Klingner, M. Baenitz, F. Steglich, *et al.*, *arXiv preprint arXiv:1806.05088* (2018).

SUPPLEMENTARY MATERIALS

TABLE S1. Crystallographic parameters of YbIr_3Ge_7 single crystals at $T = 299$ K ($R\bar{3}c$)

a (\AA)	7.8062(10)
c (\AA)	20.621(5)
V (\AA^3)	1088.2(4)
crystal dimensions (mm^3)	0.02 x 0.04 x 0.06
θ range ($^\circ$)	3.6 - 30.4
extinction coefficient	0.000107(13)
absorption coefficient (mm^{-1})	94.87
measured reflections	7380
independent reflections	374
R_{int}	0.046
goodness-of-fit on F^2	1.20
$R_1(F)$ for $F_o^2 > 2\sigma(F_o^2)^a$	0.017
$wR_2(F_o^2)^b$	0.033

$$^a R_1 = \frac{\sum ||F_o| - |F_c||}{\sum |F_o|}$$

$$^b wR_2 = \left[\frac{\sum [w(F_o^2 - F_c^2)^2]}{\sum [w(F_o^2)^2]} \right]^{1/2}$$

TABLE S2. Atomic positions, U_{eq} values, and occupancies for single crystals of YbIr_3Ge_7

Atom	x	y	z	U_{eq} (\AA^2) ^a	Occupancy
Yb	0	0	0	0.00652(14)	1
Ir	0.31885(3)	0	$\frac{1}{4}$	0.00321(11)	1
Ge1	0.54369(8)	0.68054(8)	0.03056(2)	0.0050(2)	0.970(3)
Ge2	0	0	$\frac{1}{4}$	0.0048(4)	0.911(6)

^a U_{eq} is defined as one-third of the trace of the orthogonalized U_{ij} tensor.

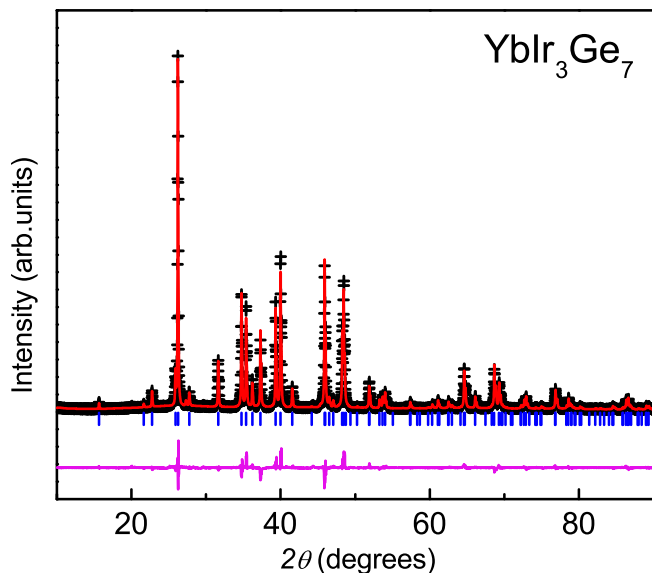


FIG. S1. Room temperature powder x-ray diffraction pattern for YbIr_3Ge_7 (black symbols) together with the calculated pattern (red line), the their difference (violet line) and calculated peak positions (blue vertical lines) using space group $R\bar{3}c$.

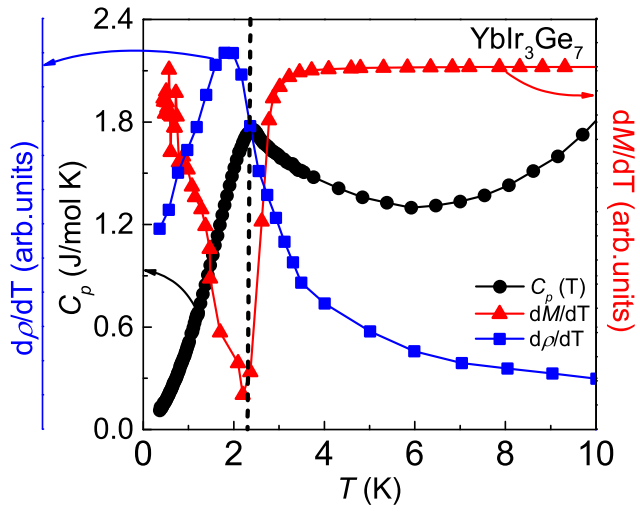


FIG. S2. The ordering temperature T_C (vertical dashed line) for YbIr_3Ge_7 determined from peaks in C_p ($H = 0$, black circles, left axis), a minimum in dM/dT ($\mu_0 H = 0.1$ T, red triangles, right axis), and $d\rho/dT$ ($H = 0$, blue squares, far left axis)